PHYSICAL REVIEW B **83**, 220103(R) (2011)

Origin of pyroelectricity in $LiNbO_3$

Qing Peng and R. E. Cohen
Geophysical Laboratory, Carnegie Institution of Washington, 5251 Broad Branch Road, NW, Washington, DC 20015, USA
(Received 15 April 2011; published 24 June 2011)

We use molecular dynamics with a first-principles-based shell model potential to study pyroelectricity in lithium niobate. We find that the primary pyroelectric effect is dominant, and pyroelectricity can be understood simply from the anharmonic change in crystal structure with temperature and the Born effective charges on the ions. This opens an experimental route to study pyroelectricity, as candidate pyroelectric materials can be studied with x-ray diffraction as a function of temperature in conjunction with theoretical effective charges. We also predict an appreciable pressure effect on pyroelectricity, so that chemical pressure, i.e., doping, could enhance the pyroelectric and electrocaloric effects.

DOI: 10.1103/PhysRevB.83.220103 PACS number(s): 77.70.+a, 31.15.xv, 71.15.Pd, 77.84.Ek

The theory of ferroelectricity had a classical period that culminated in the 1970s,[1–5] followed by a quiescent period, and was rejuvenated in the 1990s with the introduction of modern electronic structure methods to these complex, interesting, and useful materials.[6,7] The investigation of the fundamental physics of pyroelectricity, the change in polarization with respect to temperature, is difficult, as is first-principles computation of pyroelectricity, because computing properties as a function of temperature is still a big challenge. First-principles study of thermoelectromechanical properties including pyroelectricity also remains a challenge. Pioneering studies by Prosendev *et al.*[8] used an effective Hamiltonian, which requires temperature scaling of up to 60%[9] and incorrect thermal expansivity due to the neglect of hard modes. Here we use a first-principles approach that includes all degrees of freedom.

Pyroelectricity is of current great interest since the discovery of particle acceleration of ions from changes in temperature at pyroelectric surfaces sufficient to generate hard x-rays in a commercial product[10–12] as well as neutrons in heavy water via fusion.[13] There is also much interest now in the converse of the pyroelectric effect, the electrocaloric effect, for refrigeration or energy scavenging.[8,14,15] An atomic-scale understanding of pyroelectricity and the electrocaloric effect (EC) is not established, and basic questions remain: "Understanding of the mechanisms underlying the EC effect is not yet established. Three textbooks on ferroelectricity differ on the macroscopic physics of the EC effect."[16] The origin of pyroelectricity has been considered as resulting from increasing polarization disorder with temperature, but we show that is not a correct description. We find that pyroelectricity can be understood simply from the anharmonic change in crystal structure with temperature and the Born effective charges on the ions. Thus candidate pyroelectric materials can be studied with x-ray diffraction as a function of temperature in conjunction with theoretical effective charges. The classic nature of the problem is illustrated especially by attempts of Donnay to relate changes in the structure of tourmaline to its pyroelectricity (as we discuss further below), first mentioned by Theophrastus over 2300 years ago.[17,18]

$LiNbO_3$ is a uniaxial pyroelectric with space group $R3c$ in the polar phase with ten atoms per primitive cell and a T_c of 1480 K.[19] Previous density functional theory (DFT) computations for $LiNbO_3$ include frozen phonon, Berry's phase, and linear response methods.[19–21] $LiNbO_3$ has been studied experimentally extensively[1,22] due to its use in surface acoustic wave (SAW) filters and nonlinear optics.

Pyroelectricity is the change in spontaneous polarization P_s with temperature T. The total pyroelectric coefficient is

$$\Pi = \frac{dP_s}{dT} = \left(\frac{\partial P_s}{\partial T}\right)_\epsilon + \left(\frac{\partial P_s}{d\epsilon}\right)_T \left(\frac{\partial \epsilon}{\partial T}\right)_\sigma = \Pi_1 + \Pi_2. \tag{1}$$

Only changes in polarization that result in current flow are measurable or important, giving the so-called proper thermoelectromechanical coefficients. The proper pyroelectric coefficient[5] is due to the adiabatic current flow J due to a slow change in temperature, $\Pi' = \frac{dJ}{d\dot{T}}$, where $\dot{T}$ is the change in temperature T with time t. The Π' of an unclamped sample can be expressed as

$$\Pi' = \Pi_1 + \Pi_2 + \Pi_3. \tag{2}$$

The primary pyroelectric coefficient Π_1 measures the variation of spontaneous polarization with respect to temperature at constant strain (clamped), which arises from changes in phonon occupations and anharmonicity of crystals structure. The secondary effect Π_2 is the result of crystal deformation caused by thermal expansion that alters the polarization via the piezoelectric effect, $\Pi_{2i} = \alpha_{jk} c_{jklm} d_{ilm}$, where the indices label coordinate directions.[23] Repeated indices imply summation, d_{ilm} are piezoelectric compliances, c_{jklm} are elastic moduli, and α_{ij} are the thermal expansion coefficients. $\Pi_3 = 2\alpha_1 P_s$ is the difference from the total and proper pyroelectric coefficients,[1,5] where α_1 is the linear thermal expansion coefficient of the plane perpendicular to the polar axis. Π' can be measured with charge integration or dynamic pyroelectric techniques,[1] whereas it is hard to measure the components (Π_1, Π_2, Π_3) directly in experiments and they are desired in studying the pyroelectricity and its origin.

We used density functional perturbation theory (DFPT)[28] to compute phonons, effective charges, and dielectric constants. We performed first-principles calculations with the ABINIT package[29] within the local density approximation (LDA).[30] We constructed pseudopotentials using the OPIUM package[31] with an Ar core for Nb and a He core for O. We used a kinetic energy cutoff of 45 hartrees, sampled the Brillouin

zone using a $6 \times 6 \times 6$ Monkhorst-Pack mesh of k points, and results were checked against previous all-electron[19] and pseudopotential[20,21] computations. We computed the phonon frequencies using DFPT on a $4 \times 4 \times 4$ grid of q points at each of the seven volumes. The frequencies were interpolated onto a finer grid using short-range force constants.[32] Quasiharmonic Helmholtz free energies were obtained from these frequencies as functions of temperature and volume. Isotherms were fitted to the Vinet equation of state, and some results are summarized in Table I.[33] At ambient conditions we find the Born transverse effective charges to be extremely anisotropic and greatly enhanced over their nominal values [Li (Nb) xx,xy, and zz: 1.2 (7.3), 0.25 (−1.5), and 1.0 (6.4); O xx,xy,xz,yy,yz,zz: −4.2, 0.3, 1.7, −1.5, −0.1, −2.5]. The structural parameters of $LiNbO_3$ in its ground state as functions of volume were obtained by relaxing the cell shape and atomic positions at seven volumes from 92.55 to 110.19 Å^3 (−5 to 20 GPa).

The shell model approach has been proven to be accurate and computationally efficient for the simulation of ferroelectric perovskites, including bulk properties of pure crystals, solid solutions, and super lattices, and also surfaces and thin films properties.[35] In this model, each atom is represented by a massive core coupled to a massless shell, and the relative core-shell displacement describes the atomic polarization. The model contains 4th-order core-shell couplings, long-range Ewald interactions, and short-range interactions described by the Rydberg potential $V(r) = (a + br)\exp(r/\rho)$. The parameters were fit from the DFT and DFPT results of total energies, forces, stresses, phonon frequencies and eigenvectors, Born effective charges, and dielectric constants for a number of distorted and strained structures. We then performed classical molecular dynamic simulations with the DL_POLY package.[36]

We computed the spontaneous polarizations P_s during the MD simulations (Table I). The $N\sigma T$ ensemble[36] is an isothermal anisotropic constant pressure ensemble in MD simulations and it can capture the evolutions of the system volume and shape corresponding to applied pressure and temperature. The MD simulations allow us to compute dP_s/dT, the total pyroelectric coefficient Π in Eq. (1). We also performed MD simulations in the $N\epsilon T$ ensemble (constant strain) and obtained Π_1, and the difference gives Π_2. We computed Π_3 from MD $N\sigma T$ simulations.

TABLE I. First-principles calculation of structure, spontaneous polarization P_s, constant-volume specific-heat capacity C_v, and volumetric thermal expansivity α of $LiNbO_3$ using DFPT. QHLD refers to the quasiharmonic lattice dynamics calculations.

	a_H (Å)	c_H (Å)	P_s (C/m^2)	C_v (J/mol K)	α (10^{-5}/K)
DFT (0 K)	5.151	13.703	0.86		
QHLD(300 K)	5.184	13.774		94.04	3.59
MD (300 K)	5.145	13.488	0.63		2.63
Exp. (300 K)	5.151[a]	13.876[a]	0.70–0.71[b]	95.8[c]	3.24–3.83[d]

[a]Reference 24.
[b]References 1 and 25.
[c]Reference 26.
[d]References 3, 4 and 27.

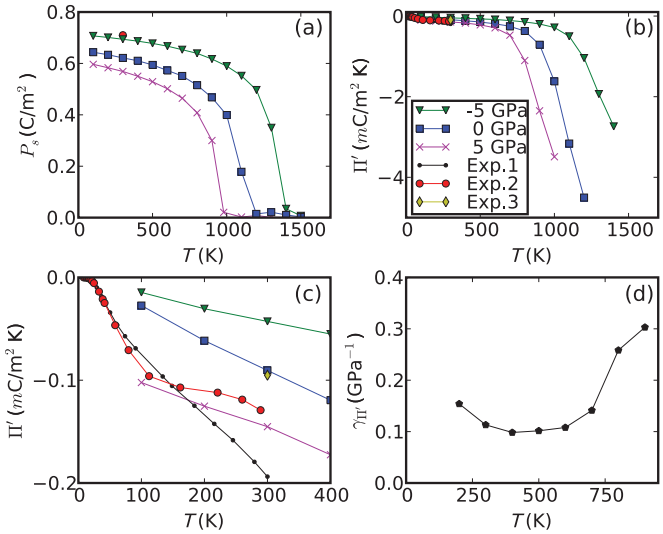

FIG. 1. (Color online) (a) Polarization and (b) proper pyroelectric coefficients for $P = -5$ (triangles), 0 (squares), and 5 (crosses) GPa. "Exp. 1, 2" labels the experimental values for a congruently melting composition and stoichiometric sample (Ref. 1), respectively; "Exp. 3" is from Ref. 37. (c) Zoom-in of (b). Our result for Π' does not go to zero at zero temperature as required by quantum mechanics since we use classical MD. (d) The pressure effect characterized by $\gamma_{\Pi'} = \frac{1}{\Pi'}\frac{\partial \Pi'}{\partial P}$.

The MD simulations were carried out in a supercell with $8 \times 8 \times 8$ primitive unit cells, giving 5120 atoms (5120 cores and 5120 shells). We find that P_s decreases with temperature and drops to zero at the phase transition to the paraelectric phase at 1200 K (Fig. 1), which agrees well with the experimental values of 1430 K[24] and 1480 K.[1] At $T = 300$ K, $P_s = 0.63$ C/m^2, and $\Pi = -107.7$ μC/m^2 K, agreeing with experiment 0.70 C/m^2 (Ref. 1) and −83 μC/m^2 K (Ref. 37), respectively. Note that the volume is underestimated with respect to experiment as a consequence of the LDA. For example, the model gave a unit cell volume of 102.89 Å^3 at room temperature, about 3.19% underestimated compared to the experimental value 106.28 Å^3 (Ref. 24). Nevertheless, the qualitative temperature behavior of polarization and pyroelectricity were correctly reproduced.

We separately computed Π_1 from MD simulations in the canonical (NVT) ensemble. The volume of the target temperature T_v was taken from the previous $N\sigma T$ simulations. MD simulations at $T = T_v$, $T_v \pm 10$, $T_v \pm 20$ K were carried out to calculate Π_1 at T_v. $\Pi_1 = -121.3$ μC/m^2 K at $T_v =$ 300 K and zero pressure, which agrees reasonably with the previous estimate of −95.8 μC/m^2 K.[23,37] Π_1 decreases with temperature and pressures, as does Π_2, calculated by $\Pi - \Pi_1$. $\Pi_2 = 13.5$ μC/m^2 K and $\Pi_3 = 17.6$ μC/m^2 K at 300 K. While lacking the direct and complete experimental data of all the coefficients of pyroelectricity, we estimate them as listed in Table II by combining the reported data of Refs. 3,4 and Ref. 1. There is good agreement between experiments and the present calculations.

As a check, we computed Π_2 from $\Pi_2 = \alpha_{jk} c_{jklm} d_{3lm} = 2e_{31}\alpha_1 + e_{33}\alpha_3$ for $LiNbO_3$, where e_{31},e_{33} are piezoelectric

TABLE II. Comparison of different contributions to the pyroelectric coefficients for $LiNbO_3$ at 300 K. Values are in units of $\mu C/m^2$ K.

	Π'	Π	Π_1	Π_2	Π_3
Present (0 GPa)	−90.2	−107.7	−121.3	13.5	17.6
Calc. from Refs. 1 and 4	−133.0	−154.9	−171.9	17.0	21.9
Exp. (Ref. 37)		−83	−95.8	12.8	

stress constants (Voigt notation), which are obtained by the first-principles calculation at zero pressure and zero temperature as listed in Table III. Using α_j obtained from $N\sigma T$ simulations, we computed Π_2 and it agrees with direct MD results at low temperatures up to 700 K.

Π_1 is dominant among the three components and Π_3 is small comparing to Π. The absolute values of both Π_1 and Π_2 increase rapidly with temperature as T_c is approached. We find that the pyroelectric effect can be understood from the changes in crystal structure with temperature, as a simple anharmonic effect. We determined the average structural parameters z, u, v, and w[21] from the average atomic positions in the MD simulations (Fig. 2). We computed the P_s versus temperature using these average positions with the Born effective charges Z^* obtained from the DFPT computations, and $P_s = \frac{e}{\Omega}\sum_i Z_i^* r_i$ where r_i is the ith ionic displacement along the polar axis from the centrosymmetric to polar structures, e the elementary charge, and Ω the unit cell volume (Fig. 2). The results show that the pyroelectric effect can be entirely understood in the classical regime above room temperature from the change in average structure with temperature, peaking at T_c.

The internal structural parameters (Fig. 2) vary with respect to temperature, giving rise to the pyroelectric effect since the ions carry effective charges. The change of these internal parameters is the measure of the internal atomic

TABLE III. First-principles calculation of the elastic moduli c, piezoelectric strain constants d, and piezoelectric stress constants e of $LiNbO_3$ using DFPT.

	Smith *et al.*[4]	Yamada *et al.*[34]	Present
c	($\times 10^{11}$ N/m^2)	($\times 10^{11}$ N/m^2)	($\times 10^{11}$ N/m^2)
c_{11}	2.030	2.03	2.18
c_{12}	0.573	0.53	0.68
c_{13}	0.752	0.75	0.78
c_{14}	0.085	0.09	0.15
c_{33}	2.424	2.45	2.40
c_{44}	0.595	0.60	0.55
c_{66}	0.728	0.75	0.75
d	($\times 10^{-11}$ C/N)	($\times 10^{-11}$ C/N)	($\times 10^{-11}$ C/N)
d_{15}	6.92	6.8	8.12
d_{22}	2.08	2.1	2.37
d_{31}	−0.09	−0.1	−0.15
d_{33}	0.60	0.6	0.81
e	(C/m^2)	(C/m^2)	(C/m^2)
e_{15}	3.76	3.7	3.72
e_{22}	2.43	2.5	2.32
e_{31}	0.23	0.2	0.22
e_{33}	1.33	1.3	1.72

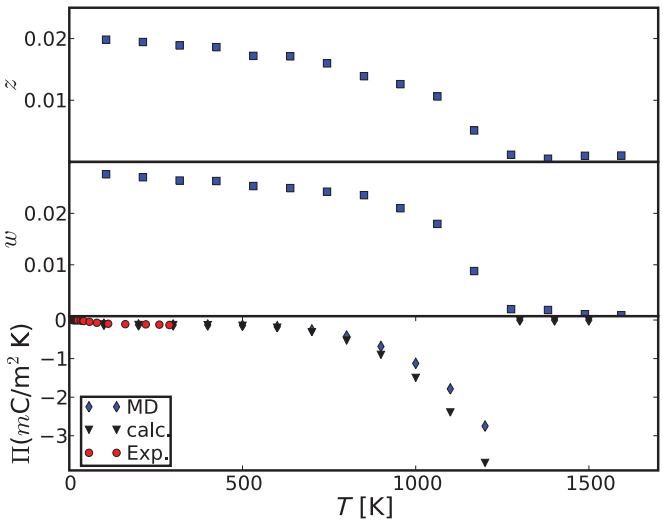

FIG. 2. (Color online) The average value of the internal structural parameters z and w (fractional displacement of Li and O along polar axis, respectively) from the MD simulations. We compare Π computed with these parameters and the Born effective charges Z^* (triangles), with experiment (circles; Ref. 1) and direct MD results (diamonds). The agreement shows that the pyroelectric effect arises almost entirely from the change in structure with temperature.

rearrangement, which associates with the anharmonic change of the crystal structure, leading to the phase transition at T_c. Thus, we can conclude that the average anharmonic internal atomic displacements with respect to the temperature contribute the dominant part of the pyroelectricity. Since these internal parameters can be obtained in experiments such as x-ray diffraction, we propose an approach to study spontaneous polarizations, pyroelectricity, and electrocaloric effect. Pyroelectric coefficients could be obtained experimentally, without electrical measurements, by studying changes in crystal structure with temperature, along with first-principles theoretical effective charges Z^*. This idea goes back at least to Donnay,[17,18] but it was not possible to resolve this quantitatively due to the small pyroelectric effect in tourmaline and other materials studied, and the lack of knowledge about appropriate effective charges. So, for example, in tourmaline, Donnay barely resolved displacements of oxygen by 0.005 ± 0.002 Å and assumed effective charges of 0.1–0.5, rather than the greatly enhanced values now known in ferroelectrics. The major advance is that now we can compute Born effective charges from first principles. Also, the displacements are much larger in ferroelectrics such as $LiNbO_3$ than in nonferroelectric pyroelectrics such as tourmaline, 55–60 times larger from room temperature to T_c in $LiNbO_3$ (for the Li and O displacements) than the value Donnay attempted to measure in tourmaline.

In order to understand the effects of pressure, we repeated the MD simulations and analysis at ±5 GPa, where volume changes −3.6% and 4.0%, T_c changes 200 K and −200 K respectively. The spontaneous polarization reduces with increasing pressure, and the pyroelectric effect is enhanced as shown in Fig. 1. The pressure effect on Π' can be characterized by $\gamma_{\Pi'} = \frac{1}{\Pi'}\frac{\partial \Pi'}{\partial P}$. Thus Π' increases by 10%–30%/GPa in

$LiNbO_3$, and increases as T_c is approached. Chemical pressure from doping would enhance the pyroelectric and electrocaloric effects.

We have used a first-principles multiscale technique, without any scaling or adjustment of parameters, to compute the pyroelectric and other thermoelectromechanical properties of $LiNbO_3$ using MD with a shell model potential fitted to DFT computations results. The pyroelectric effect increases as T_c is approached, so good pyroelectric and electrocaloric materials should have T_c only slightly higher than the operating temperatures.

This work was partly supported by the EFree, an Energy Frontier Research Center funded by the US Department of Energy, Office of Science, Office of Basic Energy Sciences under Award No. DE-SC0001057 and partly by Office of Naval Research Grant No. N00014-07-1-0451. We thank P. Ganesh and M. Rose for helpful discussions.

[1] A. M. Glass and M. E. Lines, Phys. Rev. B **13**, 180 (1976).
[2] M. E. Lines and A. M. Glass, Phys. Rev. Lett. **39**, 1362 (1977).
[3] Y. S. Kim and R. T. Smith, J. Appl. Phys. **40**, 4637 (1969).
[4] R. T. Smith and F. S. Welsh, J. Appl. Phys. **42**, 2219 (1971).
[5] J. Mangin and A. Hadni, Phys. Rev. B **18**, 7139 (1978).
[6] R. E. Cohen and H. Krakauer, Phys. Rev. B **42**, 6416 (1990).
[7] R. E. Cohen, Nature (London) **358**, 136 (1992).
[8] S. Prosandeev, I. Ponomareva, and L. Bellaiche, Phys. Rev. B **78**, 052103 (2008).
[9] L. Bellaiche, A. García, and D. Vanderbilt, Phys. Rev. Lett. **84**, 5427 (2000).
[10] J. D. Brownridge and S. Raboy, J. Appl. Phys. **86**, 640 (1999).
[11] H. Ida and J. Kawai, X-Ray Spectrom. **34**, 225 (2005).
[12] See [http://www.amptek.com/coolx.html].
[13] B. Naranjo, J. K. Gimzewski, and S. Putterman, Nature (London) **434**, 1115 (2005).
[14] J. F. Scott, Science **315**, 954 (2007).
[15] G. Akcay, S. P. Alpay, J. V. Mantese, and J. G. A. Rossetti, Appl. Phys. Lett. **90**, 252909 (2007).
[16] A. S. Mischenko, Q. Zhang, J. F. Scott, R. W. Whatmore, and N. D. Mathur, Science **311**, 1270 (2006).
[17] G. Donnay, Acta Crystallogr. Sect. A **33**, 927 (1977).
[18] G. Donnay, Can. Mineral. **23**, 655 (1985).
[19] I. Inbar and R. E. Cohen, Phys. Rev. B **53**, 1193 (1996).
[20] K. Parlinski, Z. Q. Li, and Y. Kawazoe, Phys. Rev. B **61**, 272 (2000).
[21] M. Veithen and P. Ghosez, Phys. Rev. B **65**, 214302 (2002).
[22] A. Rauber, *Current Topics in Materials Science* (North-Holland, Amsterdam, 1978), p. 481.
[23] R. E. Newnham, *Properties of Materials: Anisotropy, Symmetry, Structure* (Oxford University Press, 2005).
[24] H. Boysen and F. Altorfer, Acta Crystallogr. Sect. B **50**, 405 (1994).
[25] S. H. Wemple, J. M. DiDomenico, and I. Camlibel, Appl. Phys. Lett. **12**, 209 (1968).
[26] V. V. Zhdanova, V. P. Klyuev, V. V. Lemanov, I. A. Smirnov, and V. V. Tikhonov, Sov. Phys. Solid State **10**, 1360 (1968).
[27] *Properties of Lithium Niobate*, edited by K. K. Wong (INSPEC, 2002).
[28] P. Giannozzi, S. de Gironcoli, P. Pavone, and S. Baroni, Phys. Rev. B **43**, 7231 (1991).
[29] X. Gonze *et al*., Comput. Mater. Sci. **25**, 478 (2002).
[30] J. P. Perdew and Y. Wang, Phys. Rev. B **45**, 13244 (1992).
[31] See [http://opium.sourceforge.net].
[32] H. Kaplan, Phys. Rev. **125**, 1905 (1962).
[33] X. Sha and R. E. Cohen, Phys. Rev. B **73**, 104303 (2006).
[34] T. Yamada, N. Niizeki, and H. Toyoda, Jpn. J. Appl. Phys. **6**, 151 (1967).
[35] M. Sepliarsky, Z. Wu, A. Asthagiri, and R. E. Cohen, Ferroelectrics **301**, 55 (2004).
[36] W. Smith, C. W. Yong, and P. M. Rodger, Mol. Simul. **28**, 385 (2002).
[37] S. B. Lang, Phys. Today **58**(8), 31 (2005).